Research Article | Vol. 28, No. 2 / 20 January 2020 / Optics Express 2337
Optics EXPRESS

Comparison of interpolation-based sampling frequency offset compensation schemes for practical OFDM-VLC systems

QINGQING HU,[1] XIANQING JIN,[1,2] WEIJIE LIU,[1] DEWEN GUO,[1] MEIYU JIN,[1] AND ZHENGYUAN XU[1,3]

[1]*CAS Key Laboratory of Wireless-Optical Communications, University of Science and Technology of China, Hefei, Anhui 230027, China*
[2]*xqjin@ustc.edu.cn*
[3]*xuzy@ustc.edu.cn*

Abstract: Sampling frequency offset (SFO) is an important issue in the orthogonal frequency-division multiplexing (OFDM)-based visible light communication (VLC) systems with low-cost analog-to-digital or digital-to-analog converters (ADCs/DACs). A digital interpolation or resampling filter can be used to effectively compensate the SFO. In such case, oversampling at the receiver ADC is required to mitigate the aliasing effect due to imperfect DACs and nonlinearity of visible light sources that cause extra frequency components inside/outside the OFDM signal spectrum. The oversampling factor (rate) is mainly determined by the order of the digital interpolation filter and nonlinear VLC links. The design of the OFDM-VLC receiver incorporating the digital interpolation filter is vital as it affects not only the transmission performance but also the complexity of digital signal processing (DSP). To evaluate the feasibility of the digital interpolation-based SFO compensation schemes for cost-sensitive VLC applications, in this paper, a real-time OFDM-VLC receiver incorporating the $2^{nd}/3^{rd}/4^{th}$ order interpolation filters is experimentally demonstrated. An OFDM frame structure is designed for the synchronization including SFO estimation and compensation, in which the precision and latency of DSP are considered. On the basis of the real-time OFDM-VLC receiver, the comparison in the VLC transmission performance and DSP complexity between different interpolation-based SFO compensation schemes is discussed.

© 2020 Optical Society of America under the terms of the OSA Open Access Publishing Agreement

1. Introduction

To satisfy the ever-increasing data traffic in the current communication networks and the demand for high-speed transmission, much attention has been paid to visible light communication (VLC) in recent years. In particular, VLC has become a favorable complementary technology to millimeter-wave communication in short-range communication scenarios for future wireless networks [1–8]. For the indoor applications, as an example, it not only relieves spectral congestion in the current industrial, scientific, medical (ISM) radio band, but also provides multiple gigabit-per-second data transmission with spectral-efficient modulation techniques [2,5]. One of these techniques is orthogonal frequency-division multiplexing (OFDM) applied to improve spectral efficiency of the white light emitting diodes (LEDs)-based VLC systems [5,7]. In practice, short-range OFDM-VLC systems are cost-sensitive, in which sampling frequency offset (SFO) occurs between low-cost analog-to-digital or digital-to-analog converters (ADCs/DACs). SFO is an important issue as it causes accumulated phase rotation and severe interference between OFDM subcarriers (inter-carrier interference, ICI) [9]. Moreover, the LED nonlinearity causes extra spectral components within and beyond the OFDM signal spectrum, which affects the synchronization performance [10,11]. Although a number of methods were suggested to compensate the nonlinear distortion [12,13], most of these methods are able to

#385483 https://doi.org/10.1364/OE.385483
Journal © 2020 Received 12 Dec 2019; revised 6 Jan 2020; accepted 6 Jan 2020; published 15 Jan 2020

Optics EXPRESS

compensate the second order distortion in a practical VLC system with low complexity. Residual distortion still exists after the nonlinear compensation for a VLC link with high order nonlinear distortion. Therefore, precise synchronization is required in a cost-sensitive OFDM-VLC system.

With the rapid development of complementary metal oxide semiconductor (CMOS)-based digital electronics, high-speed hardware for digital signal processing (DSP) including DACs/ADCs has been widely used for optical communications. DSP becomes practical and attractive as it offers many advantages including flexibility and low complexity compared to traditional analog signal processing. As a result, DSP-based synchronization is a preferable option. To compensate the SFO in the digital domain, a digital interpolation or resampling filter can be used to reconstruct or resample the received signal for OFDM decoding. Prior to the DSP, the ADC usually operates at a sampling frequency (oversampling) higher than the Nyquist frequency in order to mitigate the aliasing effect due to imperfect DACs and nonlinearity of visible light sources. The oversampling factor (rate) is mainly determined by the interpolation schemes (order of the digital interpolation filter) and nonlinear VLC links. A high oversampling rate may improve the transmission performance, but increase the DSP complexity. To achieve a balance between the performance and complexity, low-level modulation formats requiring a relatively low signal-to-noise ratio (SNR) can relax the oversampling requirement as the transmission performance is tolerant of the SFO-induced ICI at a certain level. However, this results in decrease in system capacity. Therefore, it is vital to design a proper VLC receiver incorporating the digital interpolation filter, which affects not only the VLC transmission performance but also the DSP complexity.

In the literature, there is rare study about real-time investigation of OFDM synchronization for VLC applications. Most investigations in a real-time system are relevant to digital predistortion waveform shaping [14,15], equalization [16] and reduction of peak-to-average-power ratio (PAPR) [17]. In the publication [18], a training symbols-based SFO estimation was applied to compensate the phase error in a real-time laser-based VLC system, whilst the SFO-induced ICI still exists. To minimize the SFO, costly DACs/ADCs were used to achieve an SFO of approximately 12 ppm so that the SFO effect was negligible [19]. In addition, a voltage-controlled oscillator can supply an accurate frequency for the ADC [20]. However, such a method requiring extra electrical components increases the system cost and complexity.

We proposed a fourth order polynomial interpolator using the Farrow structure to digitally compensate SFO between the transmitter and receiver oscillators for VLC systems [10]. The Farrow structure has a typical property of anti-imaging for the sampling rate conversion applications when the sampling rate is increased [21]. Compared with the conventional fractional delay filter-based interpolators that require a large size lookup table for mapping a variable delay, the Farrow structure-based interpolators have advantages of low complexity and good flexibility. This is because the fixed coefficients of filters related to impulse responses are applied in the Farrow structure, whilst the only input variables are the fractional interval and integer number of samples. Experimental results with offline signal processing show that the proposed scheme can be used to effectively compensate a local frequency offset up to ± 1000 ppm at a minimum oversampling rate of 1.3 in an OFDM-based VLC system [10]. In the offline signal processing, the received signal was captured by a digital oscilloscope, in which signal recovery was carried out with Matlab. It is obvious that the precision and latency of DSP functions were not considered.

To explore the transmission performance with real-time signal processing, we further demonstrated a field-programming-gate-array (FPGA)-based OFDM-VLC receiver incorporating the synchronization function in [22], where discussions about the whole DSP design and complexity were not given. In this paper, significantly extended investigation is made on a detailed evaluation of the digital interpolation-based SFO compensation scheme with real-time DSP at the OFDM-VLC receiver. In addition, an OFDM frame structure is designed for the synchronization including

Optics EXPRESS

SFO estimation and compensation. The comparison in the VLC transmission performance and DSP complexity between different SFO compensation schemes employing a $2^{nd}/3^{rd}/4^{th}$ order interpolation filter is discussed.

2. OFDM-based VLC receiver with digital SFO estimation and compensation

2.1. Signal reconstruction with the Farrow structure-based interpolator

In a typical OFDM-VLC system with an incoherent light source (LED) as shown in Fig. 1, intensity modulation and direct detection is generally applied for short-range communications. With a DAC operating at a sampling rate of f_t, the analog OFDM signal driving the LED can be expressed as,

$$z(t) = V_b + u\sum_{k=1}^{N/2-1} Z(k)\cos(2\pi k f_t t/N) \qquad t \in [0, N/f_t] \tag{1}$$

where V_b and u are bias voltage of the LED and linear gain/attenuation of electrical components, respectively. t is a time variable. $Z(k)$ is the information data carried on the k-th subcarrier in a symbol period. N is the number of subcarriers in the positive and negative frequency range. Owing to the nonlinear transfer function of the LED for electrical-to-optical conversion, the transmitted signal is distorted seriously after the electrical-to-optical conversion. To better understand the nonlinear effect, a simplified polynomial form is used to model the LED nonlinearity [11,23]. The optical intensity of the transmitted signal can thereby be written as,

$$p(t) = \sum_{j=1}^{M} b_j z^j(t) + b_0 \tag{2}$$

where b_j is the coefficient of the j-th linear/nonlinear term. b_0 is constant and M is the highest order of the nonlinear distortion ($M \geq 2$). After light propagation over a VLC link, the received optical signal is converted by a photodiode (PD) into the electrical signal, $x(t)$, in the following form [24].

$$x(t) = p(t) \otimes h_v(t) + w(t) \tag{3}$$

$$h_v(t) = \eta e^{-2\pi k_L f_L t} u(t) \otimes e^{-2\pi k_P f_P t} u(t) \otimes h_B(t) \tag{4}$$

where h_v is linear impulse response of the VLC link including the LED, PD and electrical amplifiers. $w(t)$ is sum of shot noise and thermal noise at the receiver, which is usually modeled as additive white Gaussian noise (AWGN) [25]. η is attenuation coefficient. f_L (f_P) is the 3-dB bandwidth of the LEDs (PDs) that is modelled with a low pass filter (LPF). k_L and k_P are the fitted coefficients. $u(t)$ is the unit step function, and $h_B(t)$ is the impulse response of a high-pass filter. From Eqs. (2) and (3), new frequency components are induced within and beyond the OFDM spectrum so that the received signal spectrum is broadened widely as shown in Fig. 1.

In addition, because of the instability of the transceiver oscillators, the sampling frequency of the DAC at the transmitter may not be equal to that of the ADC at the receiver, $f_s = 1/T_s = \lambda f_t(1+\eta)$. λ is oversampling rate and η is SFO. Without proper SFO compensation in the nonlinear VLC link, the ICI and the outband frequency components cause performance degradation on the signal recovery in the OFDM decoder. Detailed description of the OFDM-VLC system with the digital SFO compensation can be found in [10]. The principle of digital SFO compensation is briefly introduced, whilst a DSP design and an OFDM frame structure for the OFDM-VLC receiver are discussed in details in this section.

The spectral aliasing effect resulted from the SFO and LED nonlinearity can be mitigated by digitally resampling the received signal with a Farrow-structured interpolator. It is noted that the digital interpolator is applied to compensate the SFO instead of the LED nonlinearity in a nonlinear VLC link. As shown in Fig. 2, the Farrow structure consists of $Q+1$ columns of finite

Optics EXPRESS

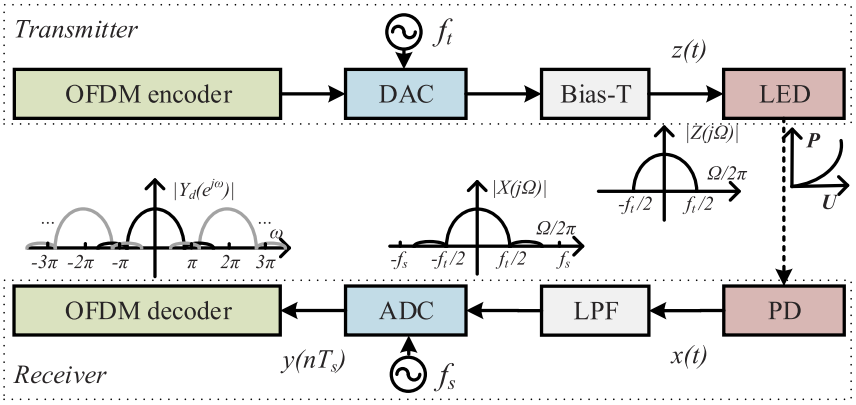

Fig. 1. Schematic diagram of a typical OFDM-VLC system with an LED-based intensity modulator.

impulse responses (FIRs) filters with K taps. In each FIR filter, fixed tap coefficients are applied. The resampled signal at an estimated sampling period (T_i) is thereby given below [26]

$$y(nT_i) = \sum_{i=0}^{K-1} x[(m_n - i)T_s] \cdot h_I[(i + \mu_n)T_s] = \sum_{q=0}^{Q} {\mu_n}^q v(q) \tag{5}$$

$$v(q) = \sum_{i=0}^{K-1} c_q(i) x[(m_n - i)T_s] \tag{6}$$

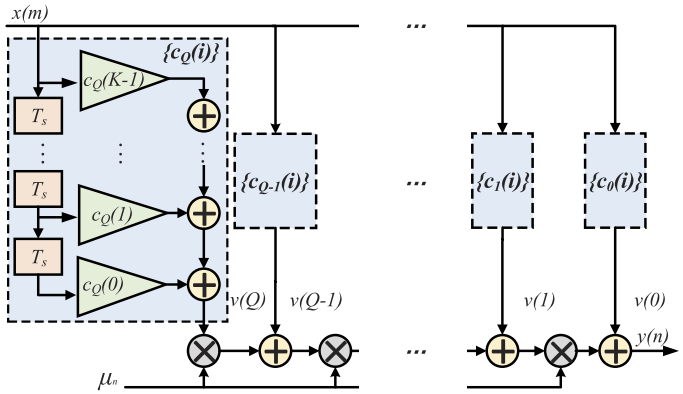

Fig. 2. A polynomial interpolator with the Farrow structure.

$c_q(i)$ is coefficient of the interpolation filter using the Farrow structure. $v(q)$ is output of the FIR filter. m_n and μ_n are input variables that determine the position of the reconstructed sample,

$$m_n = \text{int}[nT_i/T_s] = \text{int}[n\lambda(1 + \eta')] \tag{7}$$

$$\mu_n = nT_i/T_s - m_n = n\lambda(1 + \eta') - m_n \tag{8}$$

$$T_i = \lambda(1 + \eta')T_s \tag{9}$$

where the operator int[x] means the largest integer not exceeding x. μ_n is called the fractional interval specified in the interval $0 \le \mu_n < 1$. It is noted that h_I is the time-varying impulse response of the interpolation filter, which depends on the fractional interval. As the Farrow structure

Optics EXPRESS

requires only the variable μ_n for each interpolation, the precision of the interpolation mainly depends on the calculation of the μ_n. The accuracy of the μ_n is determined by the SFO estimated with pilot subcarriers, η'. Moreover, the adjustment of the μ_n in such a structure is easier than the structure of the conventional interpolation filters utilizing lookup tables.

2.2. DSP design

To design a practical VLC receiver that mitigates the SFO effect based on the aforementioned principle, a block diagram of the DSP in the OFDM-VLC receiver with the OFDM synchronization is given in Fig. 3. The digitized signal after the ADC is recovered by the DSP functions including synchronization, SFO estimation/compensation, fast Fourier transform (FFT), equalization and quadrature amplitude modulation (QAM) demapping. The synchronization function is applied to detect the start of an OFDM frame/symbol. Error vector magnitude (EVM) is calculated for quantifying the transmission performance. It is noted that as a feedback loop is applied to track the SFO estimated after the FFT, there is a delay of up to two symbol periods (FFT and SFO estimation) in compensating the SFO, which is usually not considered in the simulation or offline signal processing. This usually requires a training sequence added before the information data, which is related to the design of the frame structure to be discussed in the following part.

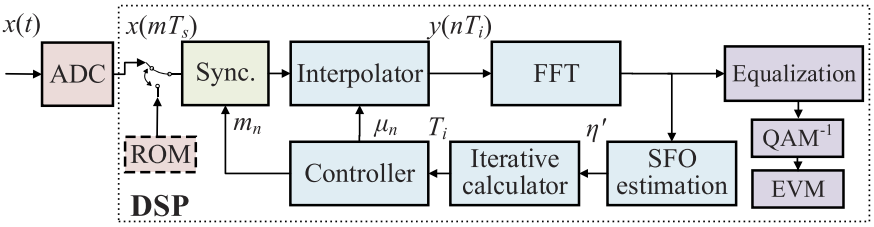

Fig. 3. Block diagram of the DSP in the OFDM-VLC receiver. Sync: synchronization.

In general, the received signal sequence including the training and information data is organized in a frame for the purposes of synchronization and channel estimation. To this end, a frame structure of the OFDM-VLC signal is designed in Fig. 4. At the beginning of each frame, a synchronization header consisting of 128 bits encoded with on-off keying (OOK) is used for the frame synchronization. As the main concern is focused on the synchronization performance, a simple zero-forcing channel estimation is applied to estimate the channel state information (CSI) with a training sequence block containing 50 OFDM symbols. The length of training symbols can be reduced with advanced channel estimation methods in practice. Following the channel estimation, the SFO is estimated with the phase difference of 4 pilot subcarriers between two OFDM symbols delayed by 4 symbols when the size of FFT is 128 [10]. To improve the estimation accuracy, a number of OFDM symbols ($\leq$40) are used to average the estimated SFO. Therefore, every 40 OFDM symbols including pilot and information subcarriers form a data block for update of the estimated SFO. Because of the relatively stable VLC channel, the number of data blocks is generally large, which is determined by the dynamic feature of the VLC links. Compared with the offline signal processing that updates the estimated SFO in each symbol period, the practical real-time signal processing has a relatively slow update rate.

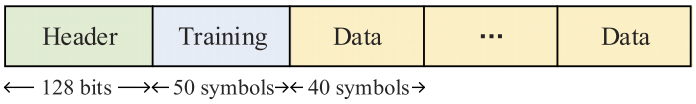

Fig. 4. Designed frame structure of the OFDM-VLC signal.

Optics EXPRESS

It is noted that to avoid the effect of imperfect ADCs, a Read Only Memory (ROM) storing simulated signals is selectively used to evaluate the DSP design of the OFDM synchronization in the VLC system. After the signal reconstruction with the Farrow-structured interpolators, normal OFDM decoding is applied. The $2^{nd}/3^{rd}/4^{th}$ order interpolation filters are considered for performance comparison in the next section.

3. Comparison in real-time transmission performance and DSP complexity

Following the discussion about the design of the OFDM-VLC receiver including the frame structure and interpolation structure for digital SFO compensation in Section 2, an FPGA-based OFDM-VLC receiver was developed to explore the feasibility of the interpolation-based SFO compensation schemes. An OFDM-VLC system as shown in Fig. 5 was established for the experimental exploration. Since the motivation of this study is to experimentally investigate the real-time performance of the SFO compensation at the OFDM-VLC receiver, an arbitrary waveform generator (AWG) was used as a transmitter for signal generation. More importantly, the application of the AWG allows us to finely adjust the sampling frequency of DAC for a specific SFO. The experimental setup of the VLC system was almost the same as that in [10] except the developed real-time OFDM-VLC receiver. The DSP design for the real-time receiver with the aforementioned synchronization algorithm was transformed to a hardware design with a DSP tool (System Generator from Xilinx). The signal recovery was conducted with the DSP on a FPGA evaluation board (Xilinx Virtex-6). Table 1 lists default values of key parameters unless explicitly mentioned.

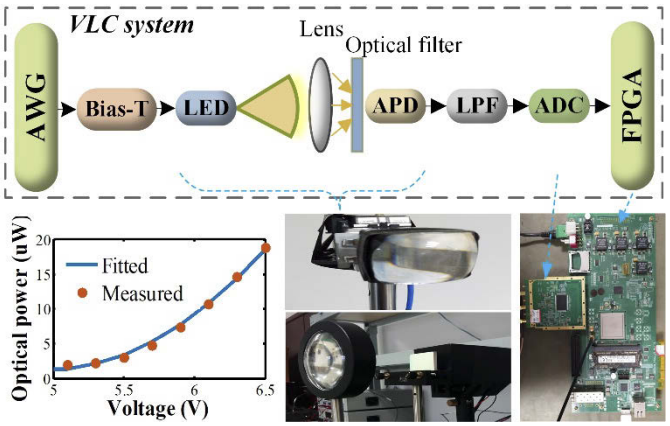

Fig. 5. Experimental setup of the OFDM-VLC system.

3.1. Verification of the DSP design

Prior to experimental investigation of the real-time transmission performance over the VLC link, experimental evaluation of the synchronization scheme was initially conducted on a single FPGA board as seen in Fig. 6. The data of the simulated OFDM signal with an arbitrary SFO was stored in the ROM as the input of the FPGA receiver. In such case, the noise in the receiver was assumed to be negligible, whilst only the SFO effect was considered. Figure 6(a) shows waveforms constructed with the 2^{nd}, 3^{rd}, 4^{th} order interpolators where SFO = 100 ppm, λ=1.3. It is clear to see that the waveform reconstructed with the 4^{th} order interpolator is closer to the waveform with SFO = 0 ppm compared with the 2^{nd} and 3^{rd} order interpolators.

To gain a good understanding of the quality of the reconstructed signal in Fig. 6(a), the statistical performance is presented in Figs. 6(b) and 6(c). The probability density functions

Optics EXPRESS

Table 1. Key parameters of the OFDM-VLC system

Parameter	Default value
Modulation format	16QAM-OFDM
Size of FFT	128
Cyclic prefix	16
Pilot subcarriers	12^{th}, 23^{rd}, 34^{th}, 45^{th}
Bias voltage (LEDs)	5.75 V
PTP of the drive signal	0.4 V
3-dB bandwidth of LEDs	6 MHz
Coefficients b_2, b_1, b_0	[0.7, -7.2, 18.0]×10^{-5}
Diameter of the lens	10 cm
Cut-off frequency (APD)	40 MHz
Photosensitive area (diameter, APD)	3 mm
Resolution of DACs (AWG)	14 bits
Resolution of ADCs	14 bits
Sampling rate (ADC)	25 or 50 MS/s
Bit rate	25.7 ~ 43.8 Mb/s
Distance	6 m

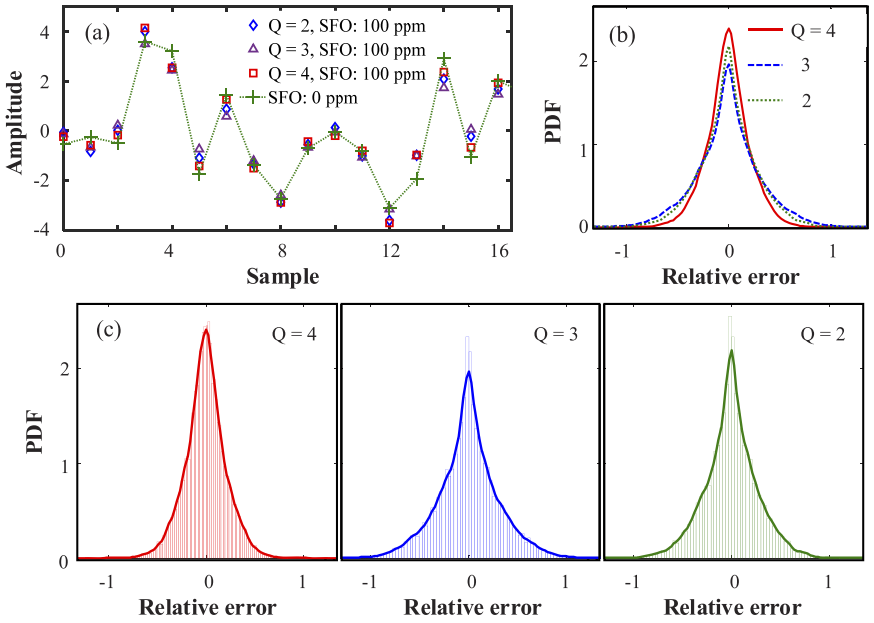

Fig. 6. (a) Waveforms constructed with the 2^{nd}, 3^{rd}, 4^{th} order interpolators. (b) Comparison of fitted PDFs, (c) PDF of reconstructed signal errors. SFO = 100 ppm, λ=1.3.

(PDFs) of the relative error of the reconstructed signal were calculated with 14,000 samples when SFO = 100 ppm. The relative error is defined as a ratio of difference between the interpolated signal and the ideal signal to the root mean square of the ideal signal. A Gaussian distribution was used to fit the measured PDF in Fig. 6(c), whilst all fitted PDF curves are plotted for comparison in Fig. 6(b). The variance of 0.042 for the 4^{th} order interpolator is smaller than that of the 2^{nd}

Optics EXPRESS

(0.071) and 3rd (0.095) order interpolators. As a result, the fitted PDF curve with the 4th order interpolator is narrower than the other interpolators. This indicates the advantage of high order interpolators for reconstruction of the OFDM signal.

Figure 7(a) shows the EVM on each subcarrier using the 4th order interpolator at different oversampling rates. Owing to the four pilot subcarriers (12th, 23rd, 34th, 45th) allocated in each OFDM symbol for the SFO estimation, only 59 subcarriers are plotted in the figure. For λ=1.0, the EVM on the high frequency subcarriers (40~59) sharply increases from -43 dB to 0 dB. This is because of the imperfect interpolation induced interference, which agrees well with the trend of the numerical result in [10]. Such high-frequency interference can be alleviated by oversampling the received signal at a relatively high frequency. It is noted that the EVM performance for λ=1.3 is close to that for λ=2.0. The best EVM performance on the subcarrier is around -46 dB, which is limited by the DSP precision depending on the designed bit width for a fractional number. Such a low EVM value facilitates application of high level modulation formats of up to 1024-QAM in theory [27,28].

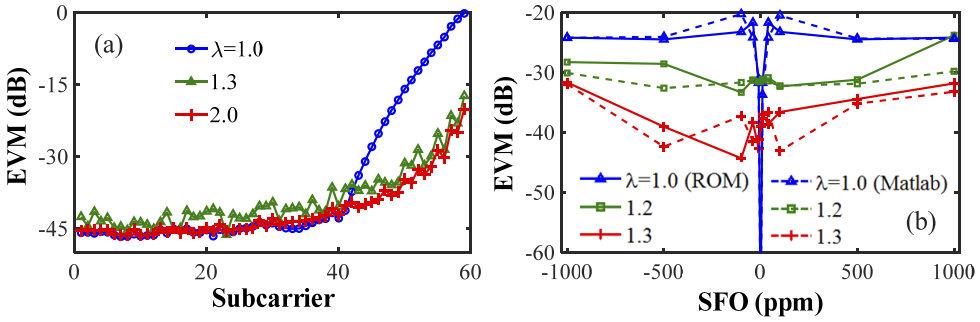

Fig. 7. (a) EVM on each subcarrier. (b) EVM comparison between simulation and experiment (ROM). Q = 4, SFO = 100 ppm.

To investigate the impact of SFO on the transmission performance, EVM as a function of SFO is shown in Fig. 7(b). The DSP function blocks at the receiver were simulated with Matlab for comparison. As seen from the figure, the EVM performance with the input signal from the ROM in the experiment is almost identical to the numerical results in the simulation (Matlab). This indicates the validity of the DSP design for the OFDM synchronization. For the perfect sampling case when SFO = 0 and λ=1, the calculated EVM is less than -50 dB. However, for nonzero values of SFO, the EVM performance increases to about -20 dB. This confirms that the EVM performance of the OFDM signal is very sensitive to SFO. As the oversampling rate is increased beyond 1.3, the EVM is improved to around -40 dB.

3.2. *Real-time VLC transmission performance*

After the verification of the synchronization schemes in a single FPGA board, experimental investigation of the real-time OFDM transmission performance was made in the VLC system in Fig. 5. At the AWG-based transmitter, a number of OFDM symbols were generated following the below procedures: 16-QAM mapping, Hermitian symmetry, inverse FFT (IFFT) and insertion of cyclic prefix. For the purpose of the OFDM synchronization, OFDM symbols were arranged according to the frame structure as shown in Fig. 4. The OFDM signal generated offline in Matlab was loaded into the AWG (Tektronix 5014C, 14-bit DAC). The SFO between the transmitter and receiver was induced by varying the sampling rate of the AWG, whilst the sampling rate of the ADC was fixed at 25 MS/s and 50 MS/s for $\lambda \neq 2$ and λ=2, respectively [10]. Because of discrete values of sampling clocks at the transmitter and receiver, the bit rate of the OFDM signal varies from 25.7 to 43.8 Mb/s. According to the measured transfer function (*P-U* curve) of the white

Optics EXPRESS

LED in Fig. 5, the bias voltage was 5.75 V, and the peak-to-peak (PTP) voltage of the driving signal was 0.4 V [29]. At the FPGA-based receiver, after optical-to-electrical conversion, the received signal is sampled by an ADC (14-bit) followed by an FPGA board for real-time signal recovery. The transmission distance was 6 m.

Figure 8 shows EVM performance using the 4th order interpolator when SFO = 100 ppm. Compared with the EVM performance from the ROM in Fig. 7(a), the EVM on the low frequency subcarriers (1-6) is relatively high due to the baseline wander effect in the low frequency range in the VLC link [24]. These low frequency subcarriers were not used for data transmission or EVM calculation. The minimum EVM is about -23 dB on the 10th subcarrier because of the attenuation and noise in the VLC link. The constellations of the received 16-QAM-OFDM signals with SFO = 100 ppm are rotated and dispersed due to the SFO-induced ICI, crosstalk and noise. After SFO compensation using the 4th order interpolator (λ=1.3), the constellation is clear, which proves the effectiveness of the SFO compensation scheme.

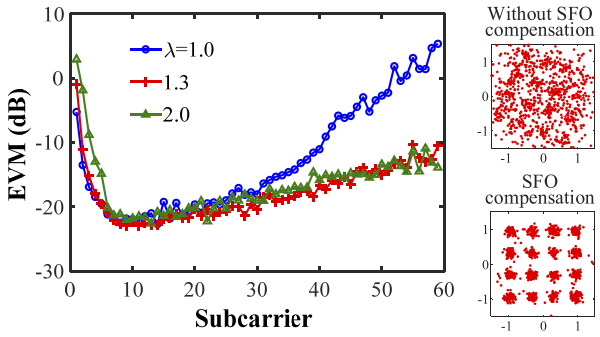

Fig. 8. EVM performance with the 4th order interpolator (SFO = 100 ppm).

Estimation of the SFO is important for the signal reconstruction because the sampling frequency of the transmitter/receiver oscillators varies with time or temperature. As an example, in Fig. 9, the estimated SFO curves are plotted when the SFO is set at around 100 ppm. Given that it is difficult to measure an accurate frequency of these oscillators, the specified SFO may not reflect a real SFO value. Therefore, the initial value of the estimated SFO is slightly higher than 100 ppm as seen in Fig. 9. After the initial estimation of SFO, the following OFDM signal is reconstructed so that the SFO estimated with the reconstructed signal is expected to be close to zero. This is confirmed in the figure that the estimated values of SFO after the first SFO estimation converge to zero. However, a small variation in SFO is observed because of the noise in the VLC link. It is noted that the magnitude of the variation in estimated SFO for λ=1.5 or 2.0 is smaller than that for λ=1.3. Because of the limited amount of samples stored in the AWG, the number of observed iterations is relatively small for large λ.

Figure 10(a) shows the measured EVM at different oversampling rates with the 4th order interpolator. All the EVM values for $\lambda \geq 1.3$ are below -16.6 dB, which corresponds to a bit error rate (BER) of 10^{-3} for 16-QAM. Compared with the offline results in [10], the EVM degrades by approximately 4 dB because of the imperfect hardware including the ADC. The EVM comparison between the 2nd, 3rd and 4th order polynomial interpolators is shown in Fig. 10(b). The EVM with the 4th order interpolator is improved by up to 1 dB compared with the low order interpolator when $\lambda = 1.3$. As the oversampling rates increases, the EVM difference between the 2nd, 3rd and 4th order interpolators becomes small. The variation in EVM for large absolute values of SFO may be because of the accumulated phase error in the channel estimation/equalization at a relatively slow update rate of estimated SFO. Such variation can be minimized by applying advanced channel equalization algorithms, which is beyond the scope of this study.

Optics EXPRESS

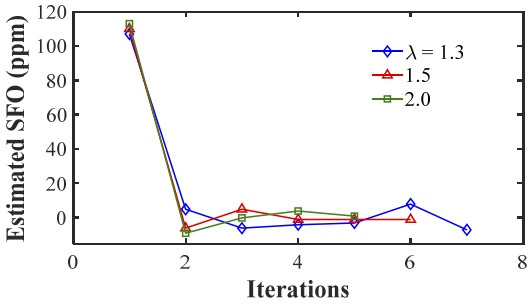

Fig. 9. Estimated SFO with the 4th interpolator at different oversampling rates (λ).

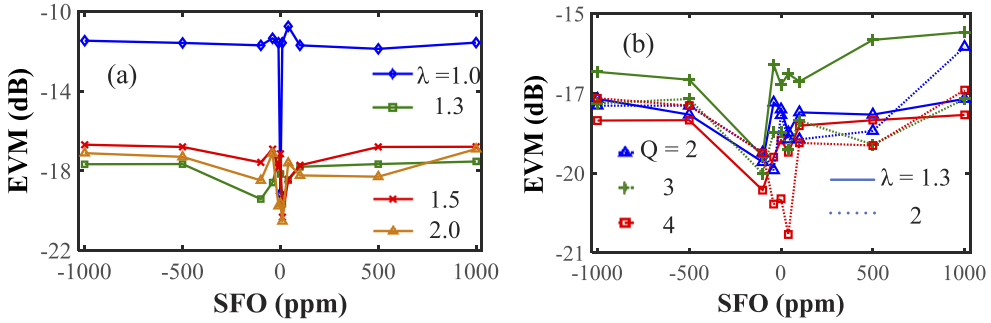

Fig. 10. (a) Measured EVM versus SFO ($Q = 4$), (b) EVM performance with the 2nd, 3rd and 4th order interpolators.

Table 2 shows the DSP complexity of different interpolators in the report of the hardware compilation for the DSP design. The consumed resources of hardware and latency increase with the order of the digital interpolator. Compared with the 2nd order interpolator, the consumed resources for the 3rd order interpolator are increased by at least 50%, whilst the 4th order interpolator almost doubles the latency. In general, the DSP complexity for the 4th order interpolator increases by a factor of 2 to 7. The consumed DSP48E, slice registers and logic resources (slice LUTs, occupied slices and LUT flip-flop pairs) are about 2, 3, and 4 times that for the 3rd order interpolator, respectively. As a result, a high order digital interpolator can be used to effectively compensate SFO at the cost of DSP complexity, which however results in a reduced oversampling rate of ADC. This can relax the requirement for ADCs in terms of sampling speed and stability of the oscillators. Moreover, the consumed resources takes a small amount of the whole available sources on the FPGA board. Therefore, high order digital interpolators are still

Table 2. Comparison in DSP complexity of the Farrow-structured interpolators

Resource	Available	$Q = 2$	$Q = 3$	$Q = 4$
Slice LUTs	80,000	611	1020	4388
Slice registers	160,000	631	932	2798
Occupied slices	20,000	190	336	1479
LUT flip-flop pairs	18,300	694	1159	4591
DSP48E	480	5	9	18
Latency (sample period)	-	9	12	17

Optics EXPRESS

promising solution for future VLC applications as modern digital electronics grows fast in recent years.

4. Conclusion

A real-time OFDM-VLC receiver incorporating the designed digital interpolation-based SFO compensation has been successfully demonstrated with commercially available LEDs and DACs/ADCs. It has shown that based on a designed OFDM frame structure the real-time OFDM transmission performance with the $2^{nd}/3^{rd}/4^{th}$ order Farrow-structured interpolator is robust to SFO up to ± 1000 ppm. A trade-off between the DSP complexity and oversampling rate at the receiver has been recognized. Compared with the low order interpolators, the EVM with the 4^{th} order interpolator is improved by up to 1 dB, whilst the DSP complexity increases by a factor of 2 to 7. Moreover, the consumed hardware resources take a small amount of the whole available sources on the FPGA board, which makes the high order digital interpolator-based SFO compensation promising for future short-range VLC applications. In addition, it has been observed that the latency of DSP results in a relatively slow update rate of estimated SFO, which may affect the EVM performance for large SFO. The optimization of the DSP latency related to estimation of SFO and CSI will be studied in the future.

Funding

National Key Research and Development Program of China (2017YFB0403604); National Natural Science Foundation of China (61631018, 61971394); Key Research Program of Frontier Sciences of Chinese Academy of Sciences (QYZDY-SSW-JSC003); Fundamental Research Funds for the Central Universities (WK2100060022).

Acknowledgement

The authors would like to thank Information Science Laboratory Center of USTC for the hardware and software services.

Disclosures

The authors declare no conflicts of interest.

References

1. H. Elgala, R. Mesleh, and H. Haas, "Indoor optical wireless communication: potential and state-of-the-art," IEEE Commun. Mag. **49**(9), 56–62 (2011).
2. Y. Wang, X. Huang, J. Zhang, Y. Wang, and N. Chi, "Enhanced performance of visible light communication employing 512-QAM N-SC-FDE and DD-LMS," Opt. Express **22**(13), 15328–15334 (2014).
3. P. Pathak, X. Feng, P. Hu, and P. Mohapatra, "Visible light communication, networking, and sensing: a survey, potential and challenges," IEEE Commun. Surv. Tutorials **17**(4), 2047–2077 (2015).
4. Z. Ghassemlooy, S. Arnon, M. Uysal, Z. Xu, and J. Cheng, "Emerging optical wireless communications-advances and challenges," IEEE J. Select. Areas Commun. **33**(9), 1738–1749 (2015).
5. S. Rajbhandari, H. Chun, G. Faulkner, K. Cameron, A. Jalajakumari, R. Henderson, D. Tsonev, M. Ijaz, Z. Chen, H. Haas, E. Xie, J. McKendry, J. Herrnsdorf, E. Gu, M. Dawson, and D. O'Brien, "High-speed integrated visible light communication system: device constraints and design considerations," IEEE J. Select. Areas Commun. **33**(9), 1750–1757 (2015).
6. L. Feng, R. Hu, J. Wang, P. Xu, and Y. Qian, "Applying VLC in 5G networks: architectures and key technologies," IEEE Network **30**(6), 77–83 (2016).
7. M. Mohammed, C. He, and J. Armstrong, "Mitigation of side-effect modulation in optical OFDM VLC systems," IEEE Access **6**, 58161–58170 (2018).
8. T.-C. Wu, Y.-C. Chi, H.-Y. Wang, C.-T. Tsai, C.-H. Cheng, J.-K. Chang, L.-Y. Chen, W.-H. Cheng, and G.-R. Lin, "White-lighting communication with a $Lu_3Al_5O_{12}:Ce^{3+}$/$CaAlSiN_3:Eu^{2+}$ glass covered 450-nm InGaN laser diode," J. Lightwave Technol. **36**(9), 1634–1643 (2018).

Optics EXPRESS

9. X. Wang, T. Tjhung, Y. Wu, and B. Caron, "SER performance evaluation and optimization of OFDM system with residual frequency and timing offsets from imperfect synchronization," IEEE Trans. Broadcast. **49**(2), 170–177 (2003).
10. Q. Hu, X. Jin, and Z. Xu, "Compensation of sampling frequency offset with digital interpolation for OFDM-based visible light communication systems," J. Lightwave Technol. **36**(23), 5488–5497 (2018).
11. I. Neokosmidis, T. Kamalakis, J. Walewski, B. Inan, and T. Sphicopoulos, "Impact of nonlinear LED transfer function on discrete multitone modulation: analytical approach," J. Lightwave Technol. **27**(22), 4970–4978 (2009).
12. G. Stepniak, J. Siuzdak, and P. Zwierko, "Compensation of a VLC phosphorescent white LED nonlinearity by means of volterra DFE," IEEE Photonics Technol. Lett. **25**(16), 1597–1600 (2013).
13. Y. Wang, L. Tao, X. Huang, J. Shi, and N. Chi, "Enhanced performance of a high-speed WDM CAP64 VLC system employing volterra series-based nonlinear equalizer," IEEE Photonics J. **7**(3), 1–7 (2015).
14. P. Thai, "Real-time 138-kb/s transmission using OLED with 7-kHz modulation bandwidth," IEEE Photonics Technol. Lett. **27**(24), 2571–2574 (2015).
15. W. Xu, M. Zhang, D. Han, Z. Ghassemlooy, P. Luo, and Y. Zhang, "Real-time 262-Mb/s visible light communication with digital predistortion waveform shaping," IEEE Photonics J. **10**(3), 1–10 (2018).
16. Y. Xue, Y. Hou, S. Xiao, Y. Zhang, and L. Zhang, "Real-time visible light communication system based on 2ASK-OFDM coding," in *Proc. of Opto-Electronics and Commun. Conf.*, 1–3 (2016).
17. Y.-L. Gao, Z.-Y. Wu, Z.-K. Wang, and J. Wang, "A 1.34-Gb/s real-time Li-Fi transceiver with DFT-spread-based PAPR mitigation," IEEE Photonics Technol. Lett. **30**(16), 1447–1450 (2018).
18. R. Deng, J. He, M. Chen, Y. Wei, J. Shi, and L. Chen, "Real-time VLLC-OFDM HD-SDI video transmission system with TS-based SFO estimation," in *Proc. of Opt. Fiber Commun. Conf.*, W1 K.6 (2017).
19. R. Deng, J. He, Z. Zhou, J. Shi, M. Hou, and L. Chen, "Experimental demonstration of software-configurable asynchronous real-time OFDM signal transmission in a hybrid fiber-VLLC system," IEEE Photonics J. **9**(1), 1–8 (2017).
20. M. Chen, J. He, Z. Cao, J. Tang, L. Chen, and X. Wu, "Symbol synchronization and sampling frequency synchronization techniques in real-time DDO-OFDM systems," Opt. Commun. **326**, 80–87 (2014).
21. J. Vesma and T. Saramäki, "Polynomial-based interpolation filters-part I: Filter synthesis," Circuits Syst. Signal Process **26**(2), 115–146 (2007).
22. Q. Hu, X. Jin, W. Liu, M. Jin, and Z. Xu, "Real-time OFDM receiver with robust frequency synchronization for visible Light communication," in *Proc. of Asia Commun. and Photonics Conf.*, T2B.3 (2019).
23. J. Li, Z. Huang, X. Liu, and Y. Ji, "Hybrid time-frequency domain equalization for LED nonlinearity mitigation in OFDM-based VLC systems," Opt. Express **23**(1), 611–619 (2015).
24. Y. Mao, X. Jin, W. Pan, W. Liu, M. Jin, C. Gong, and Z. Xu, "Real-time investigation of CAP transceivers with hybrid digital equalization for visible light communication," Opt. Express **27**(7), 9382–9393 (2019).
25. A. Cailean, B. Cagneau, L. Chassagne, V. Popa, and M. Dimian, "Evaluation of the noise effects on visible light communications using Manchester and Miller coding," in *Proc. of International Conf. on Develop. & App. Systems*, 85–89 (2014).
26. L. Erup, F. Gardner, and R. Harris, "Interpolation in digital modems-part II: Implementation and performance," IEEE Trans. Commun. **41**(6), 998–1008 (1993).
27. S. Kawai, T. Yamagishi, Y. Hagiwara, S. Saigusa, I. Seto, S. Otaka, and S. Ito, "A 2018-QAM capable WLAN receiver with -56.3 dB image rejection ratio using self-calibration technique," IEICE Trans. Electron. **E101C**(7), 457–463 (2018).
28. M. Xu, Z. Jia, J. Wang, L. Campos, and G.-K. Chang, "A novel data-compression technology for digital mobile fronthaul with Lloyd algorithm and differential coding," in *Proc. of Opt. Fiber Commun. Conf.*, Tu2K-2 (2018).
29. R. Yang, X. Jin, M. Jin, and Z. Xu, "Experimental investigation of optical OFDMA for vehicular visible light communication," in *Proc. of European Conf. on Opt. Commun.*, 1–3 (2017).

112.32.34.241 {ts '2020-02-26 22:14:46'}